

RECENT RESULTS FROM ICECUBE ON NEUTRINOS AND COSMIC RAYS

S.BÖSER for the ICECUBE collaboration^a
Physikalisches Institut, Universität Bonn, Nußallee 12
53115 Bonn, Germany

Encompassing a volume of $\sim 1 \text{ km}^3$ of glacial ice at the South Pole, ICECUBE is currently the worlds largest neutrino detector. It consists of 5160 optical modules on 86 strings in a depth between 1450 m and 2450 m, as well as 324 optical modules arranged in 81 stations on the surface to detect charged cosmic rays. A large amount of data has already been acquired with smaller configurations throughout the installation period.

Using this data the atmospheric neutrino spectrum in the northern hemisphere has been measured up to 100 TeV. No point sources have been identified in a set of more than 10^5 neutrino candidates from both hemispheres. Searches for transient sources have set stringent limits on neutrino emission from gamma-ray bursts, and are now accompanied by an extensive neutrino-triggered follow-up program. A very large statistics of cosmic ray events has revealed an anisotropy in the cosmic ray flux on the 10^{-3} level in the 10 – 100 TeV range. While no sources of extra-terrestrial neutrinos have been found yet, the physics results obtained so far illustrate the very good performance of the detector.

1 Introduction

The ICECUBE detector depicted in Figure 1 employs the $\sim 3 \text{ km}$ thick glacial ice cap at the South Pole as a target for neutrino-nucleon interactions. The emerging high-energetic charged particles emit Cherenkov light that is detected by optical modules embedded in the ice. Each optical module consists of a photomultiplier tube in a pressure housing¹. In its now final configuration a total of 86 strings holding 60 modules each has been deployed throughout seven consecutive polar seasons from 2004 to 2011. To distinguish the data sets that have been acquired throughout this construction phase, the different configurations are denoted by the numbers of strings (e.g. IC59 for the 59-string setup completed in 2010).

With a horizontal spacing of 125 m and a vertical sensor spacing of 17 m on the majority of strings, the best sensitivity is achieved for neutrino-induced muons above $\sim 100 \text{ GeV}$. In the center of the array, the denser spaced DEEPCORE array, yields a lower muon threshold of $\sim 10 \text{ GeV}$. Waveforms of the PMT's pulse from the Cherenkov photons are digitally captured and timestamped with $< 3 \text{ ns}$ precision before being transmitted to the surface, where the data is filtered and transmitted north via satellite. Using a likelihood method based on detailed modeling of the optical scattering and absorption properties of the ice², the Cherenkov cone of the muon traversing the ice can be reconstructed. This reconstructed direction is used as a primary discriminator between the abundant flux of atmospheric muons from cosmic ray air-showers from above the detector and muons induced by neutrinos interacting in the ice or bedrock below the detector.

^a<http://www.icecube.wisc.edu>

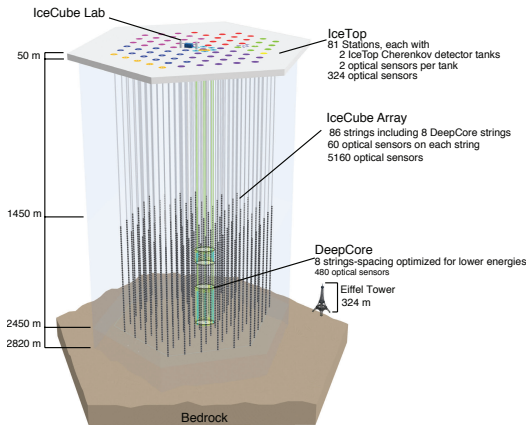


Figure 1: Schematic view of the ICECUBE detector with the subdetectors DEEPCORE and ICETOP.

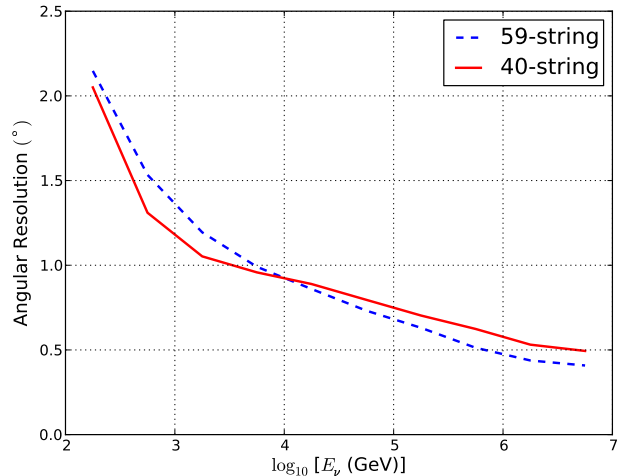


Figure 2: Median neutrino angular resolution for ν_μ as a function of true neutrino energy for a cut-based (IC40) and boosted decision tree-based (IC59) analysis³.

Despite the scattering of the Cherenkov light in the ice, good pointing can be achieved due to the length of the muon track in the detector. The resulting angular resolution for ν_μ (including the ν - μ scattering angle of $\langle\theta_{\nu\mu}\rangle \approx 1^\circ/\sqrt{E_\nu/\text{TeV}}$) obtained from simulation as achieved in a point-source analysis with ICECUBE is shown in Figure 2. Typically an accuracy of $\sigma_\theta(\nu_\mu) \approx 1^\circ$ deg is achieved at $E_\nu = 1$ TeV. The accuracy of the resolution as well as the absolute pointing has been verified by observation of the moon shadow in cosmic-ray induced muons³, which has now been observed with more than 13σ . The energy of the neutrino has to be estimated from the energy loss of the muon, which is increasingly dominated by stochastic processes at higher energies, and is thus limited to $\sigma_E(\mu) \sim 0.3 \log_{10}(E_\mu)$. The muon energy yields only a very coarse proxy for the neutrino energy which is only partially transferred to the muon (that is also typically not contained in the detector). For ν_e -induced cascades that are fully contained in the detector, a much better energy resolution of $\sigma_E(\nu_e) \sim 0.13 \log_{10}(\nu_e)$ is achieved, albeit at an order of magnitude lower effective area.

This INICE part of the observatory is augmented by a 1 km^2 air-shower detector ICETOP on top of the array. 324 of the same optical modules are placed in pairs in ice filled tanks of 2 m diameter, two of which are placed above every string. This geometry provides a combined aperture of $A_{\text{eff}} \cdot \Omega = 0.3 \text{ km}^2 \text{ sr}$ that yields about 10^7 events per year above 300 TeV coincidentally detected in the INICE and ICETOP part of the array.

2 Neutrinos

The detection of extra-terrestrial high-energy neutrinos is the main objective of ICECUBE. Through the interactions of protons with ambient matter $p + N \rightarrow \pi^{\pm/0} + X$ or radiations fields $p + \gamma \rightarrow \Delta^+ \rightarrow \pi^{\pm/0} + p/n$ and subsequent decay of the pions $\pi^0 \rightarrow \gamma\gamma$ and $\pi^\pm \rightarrow \mu^\pm + \nu_\mu/\bar{\nu}_\mu \rightarrow e^\pm + \nu_e/\bar{\nu}_e + \nu_\mu/\bar{\nu}_\mu$ the sources of high-energy cosmic rays are intimately linked to high-energy photons and neutrinos.

2.1 Point Sources

While charged cosmic rays are scattered in intergalactic magnetic fields and photons are easily absorbed on the interstellar radiation fields or the cosmic microwave background, neutrinos can free-stream from the sources, and reveal their identity by a flux enhancement from that particular direction. Figure 3 shows a skymap of arrival directions of neutrino candidates. The plot contains 57460 up-going and 87009 down-going neutrino candidates selected from 723 days of data taken

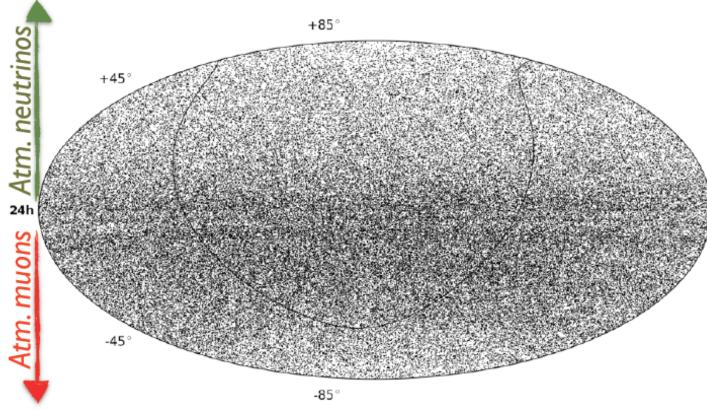


Figure 3: Skymap of neutrino candidates in equatorial coordinates for IC40+IC59. The curved line indicates the galactic plane.

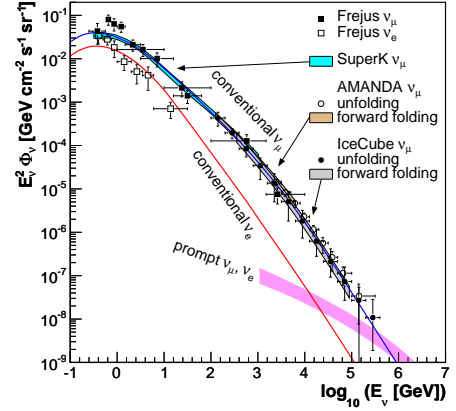


Figure 4: Spectrum of atmospheric neutrinos from unfolding of the IC40 data set⁵.

with IC40 and IC59. In the Northern sky it is dominated by atmospheric neutrinos. As the flux of atmospheric muons falls with a much steeper spectral index of -3.7 than anticipated from a neutrino source, this search can be extended to the Southern sky by raising the energy threshold with zenith angle.

In a fine-binned full-sky likelihood analysis incorporating the number of likely signal events as well as a spectral index for each point the hottest spot at $(\text{Ra}, \text{Dec}) = (75.45^\circ, 8.15^\circ)$ has a pre-trial p-value of $p = 2.23 \cdot 10^{-5}$ and a post-trial p-value of 0.67, indicating a high compatibility with the null hypothesis³. The resulting zenith-dependant limit on neutrino fluxes from point sources not only exceeds the initial sensitivity expected for the full detector configuration, but also poses competitive limits in the Southern hemisphere. In addition, limits on the neutrino emission are derived for a list of preselected source candidates³. No significant point source has been observed in either search.

2.2 Diffuse neutrino flux

Following an analytic approximation⁴, the flux of atmospheric neutrinos can be approximated as a sum over the meson decay channels $\phi_\nu(E_\nu) = \phi_N(E_\nu) \sum_{\pi, K, D, \Lambda_c, \dots} \frac{A_i}{1 + B_i \cos \theta E_\nu / \epsilon_\nu}$ where $\phi_N(E_\nu)$ is the primary spectrum of nucleons evaluated at the energy of the neutrino and θ is the zenith angle at the effective production height. The most important contribution to at TeV energies is the "conventional" flux from $K^\pm \rightarrow \mu^\pm + \nu_\mu / \bar{\nu}_\mu$ and a smaller contribution from $\pi^\pm \rightarrow \mu^\pm + \nu_\mu / \bar{\nu}_\mu$. As the neutrino energy increases above the critical energy $\epsilon_i / \cos \theta$ ($\epsilon_\pi \sim 110 \text{ GeV}$, $\epsilon_K \sim 820 \text{ GeV}$), the spectrum steepens – asymptotically by one power of energy with respect to the primary spectrum. Since the muon carries an unknown fraction of the neutrino energy, a complex deconvolution mechanism has to be employed to infer the spectrum. Figure 4 shows the result of an unfolding of the IC40 data of downgoing neutrinos. While the contribution of the "prompt" neutrino flux from the decays of charmed mesons is significantly smaller in the TeV-regime, the critical energy is in the order of 10^7 GeV . Hence their contribution will follow the primary spectral index of the charged cosmic rays over the sensitivity range of ICECUBE and they will become the dominated flux in the PeV-regime, which is expected to be accessible with the full statistics of the completed detector.

2.3 Gamma Ray Bursts

In the fireball model, GRBs are modeled as explosions of very massive stars which eventually collapse to a black hole. In such models the observed gamma rays stem from synchrotron radiation and/or inverse Compton scattering of electrons accelerated in shock fronts in the collimated explosive outflow. It was proposed that in the same way also protons are accelerated^{6,7}. These

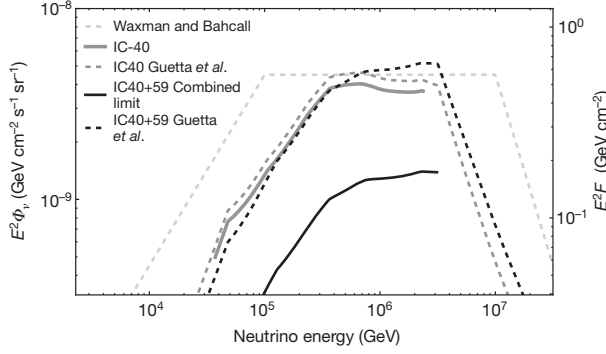


Figure 5: 90% C.L. upper limits (solid lines) on the neutrino fluxes from GRBs set IC40 and IC59¹¹ with respect to the flux expected from the model of Guetta et al.⁹ (dashed lines). The Waxman–Bahcall flux¹⁰ assumes an average shape of the GRB spectra.

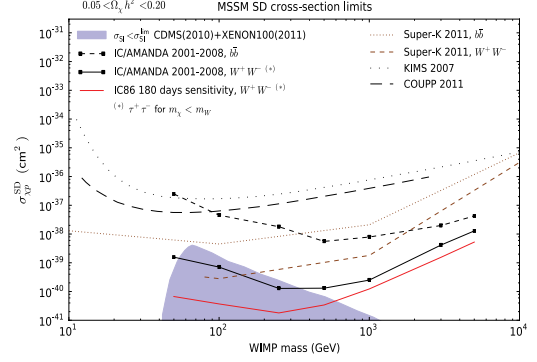


Figure 6: Limit on the WIMP-induced muon flux for annihilation to $b\bar{b}$ (black dotted) and W^+W^- (black) as well as the predicted sensitivity for IC86 (red). The shaded area shows the allowed MSSM parameter region with constraints from CDMS and XENON¹⁵.

protons would undergo interactions with the surrounding photon field in the fireball and thus generate neutrinos^{7,9}.

In a search for neutrinos from GRBs using the IC40 and IC59 detector configurations, 224 GRBs reported by the GCN in the northern sky have been selected. A likelihood was derived using a flat arrival time prior inbetween the first and last photon observed for each GRB (typically $\Delta t = 0.1 - 100$ s). The estimated pointing resolution is taken into account for the neutrino direction from ICECUBE as well as the GRB position. No neutrino event has been observed against an expectation of 8.4 events from the prompt phase model⁹ with neutrino spectra calculated from the observed photon spectrum for each GRB individually⁸. Figure 5 shows the predicted neutrino flux as a function of energy for an average model¹⁰ as well as for the specific set of GRBs entering the analysis, together with the flux limit derived using the IC40, IC59 and combined IC40+IC59 dataset¹¹.

2.4 ICECUBE's Follow-up Program

While ICECUBE continuously monitors the full northern hemisphere with a typical uptime of above 99%, most optical, X-ray and γ -ray detectors have significantly smaller fields of view and/or duty-cycles. In order to increase the coincident observation time, a number of neutrino-triggered follow-up programs have been setup. In an online-analysis chain, neutrino candidates are extracted from the data flow at the South Pole with a latency of a ~ 6 min and a purity of $> 70\%$, from which alerts are generated and forwarded to the northern hemisphere via a satellite connection.

- In the **Optical follow-up** deviations from the atmospheric neutrino flux are identified by searching for multiplets within a time window of $\Delta t < 100$ s and angular distance $\Psi < 3.5^\circ$. Based on a likelihood criterion incorporating the temporal and spatial distance as well as the angular resolution, alerts are forwarded to the optical telescopes ROTSE and PTF. A first analysis¹² using data from Dec. 2008 to Dec. 2009 yields an insignificant 2.1σ -excess of multiplets. No supernova has been identified in 17 follow-up observations with ROTSE. For the first time a dedicated search set stringent limits on models for choked jets in core-collapse supernovae¹³. Since Mar. 2011, the program has been extended by an **X-ray follow-up** with the SWIFT satellite, aiming at the observation of the rapidly decaying afterglow from GRBs.

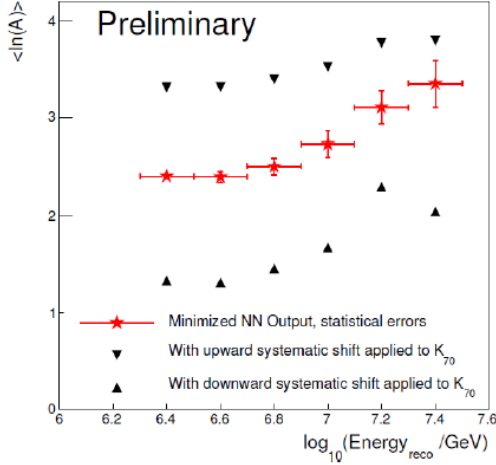


Figure 7: Average logarithmic mass of cosmic rays from one month of data with IC40/IT40¹⁷.

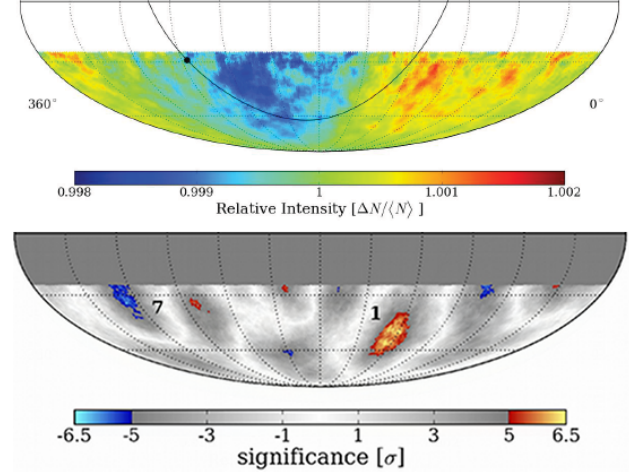


Figure 8: Relative intensity map for cosmic rays of the 20 TeV sample (top) and excess significance after subtraction of the dipole and quadrupole component (bottom)¹⁷.

- For the γ -ray follow-up³ a set of 109 source candidates (predominantly AGNs) is identified a-priori. A time-clustering algorithm searches for excesses from these directions in the online neutrino stream within time scales of up to 3 weeks, taking into account the temporal variability of the background. Alerts from this program will be sent to the MAGIC and VERITAS γ -ray telescopes with an expectation of one background-induced alert/year.

2.5 WIMP searches

It is speculated that WIMPs can lose energy through elastic scattering with ordinary matter, and become trapped in gravitational wells. The accumulated excess gives rise to an increased annihilation rate, resulting in turn in a neutrino flux enhancement from decay of the self-annihilation products. ICECUBE is hence looking for neutrinos from WIMP annihilation by searching for enhanced signals from the Earth's center¹⁴, the Sun¹⁵ or the galactic halo¹⁶. By assuming that in the Sun an equilibrium between capture and annihilation is reached, the neutrino-induced muon flux can be related to the spin-dependant cross-section σ_{SD} . In Figure 6 limits for σ_{SD} are given for WIMP masses m_χ from 50 GeV to 5 TeV¹⁶. As the effective area of ICECUBE increases with energy, its sensitivity will depend on the spectrum of the decay products. Hence significantly stronger constraints can be placed on the decay $\chi\chi \rightarrow W\bar{W}$ compared to $\chi\chi \rightarrow b\bar{b}$. This analysis combines data taken with ICECUBE and the precursor detector AMANDA between 2001 and 2008, with a total livetime of 1065 days when the Sun was below the horizon¹⁶.

The shaded area in Figure 6 indicates the region not yet excluded by the MSSM parameter constraints through the direct searches by the experiments CDMS and XENON100. Comparing with the expected sensitivity for a livetime of 180 days for the full detector also shown in Figure 6 illustrates the potential of the approach.

3 Cosmic Rays

3.1 Spectrum and composition

For measuring cosmic rays, ICECUBE is complemented by the surface air shower array ICETOP, which samples the electromagnetic shower component, whereas the deep detector responds to punch-through muons from the hadronic shower component. This combination offers a unique possibility to determine the spectrum and mass composition of cosmic rays from about 300 TeV to 1 EeV. The first analysis exploiting this correlation¹⁷ uses a small data set corresponding to only one month of data taken with about a quarter of the final detector. A neural network

was employed to simultaneously determine the primary energy and mass from the measured input variables shower size and muon energy. The resulting average logarithmic mass shown in Figure 7 indicates that the average mass of the primary particles increases with energy in the knee region around 10^{15} eV¹⁷.

3.2 Cosmic Ray anisotropy

A large sample of 10^{11} cosmic ray muon events has been collected by ICECUBE between 2007 and 2010 (and will roughly increase by the same amount every year with the full detector). For the first time, the anisotropies previously reported on multiple angular scales^{19,20} could be studied in the Southern sky as well^{21,22}. In a multipole analysis, a dominant dipole contribution is found that does not coincide with the direction of the Compton-Getting effect¹⁸, indicating that the cosmic rays co-rotate with the local galactic magnetic field. Additional structures are found on angular scales from $15 - 30^\circ$ (c.f. Figure 8). These are potentially ascribed to the local magnetic field and source configuration, and may hence carry key information on the origin of galactic cosmic rays.

3.3 Future enhancements

It has been shown recently that air-showers can also be detected by the coherent radio emission in the $10 - 100$ MHz regime²³ dominantly stemming from deflection of the electrons in the earth magnetic field and a net charge excess in the shower^{24,25}. In contrast to ICETOP which samples the shower on the ground, the basically unattenuated radio signal reflects the integral development of the shower through the atmosphere, and might additionally yield an independent handle on the shower maximum²⁶. It has hence been suggested²⁷ that complementing the ICECUBE observatory with an array of radio receivers could contribute significantly to a precise measurements of the cosmic ray spectrum and composition. Results from a first test setup²⁸ indicate very low ambient noise levels at the South Pole and therefore the good suitability of the location for this approach.

4 Conclusion

While no extra-terrestrial sources of neutrinos have been identified yet, the physics results obtained with ICECUBE throughout the construction period demonstrate the excellent performance. The increased statistics available with the now complete detector and continuous improvements in reconstruction and background rejection propose ICECUBE will continue to make key contributions to a wide class of physics cases in the future.

References

1. K. Hanson *et al.*, *NIM A* **567**, 214 (2006)
2. K. Woschnag *et al.*, Conf. Proc. C **990817V2** (1999)
3. R. Abbasi *et al.*, ICRC (2011) arXiv:1111.2741
4. P. Lipari, *Astrop. Ph.* **1**, 195 (1993)
5. R. Abbasi *et al.*, ICRC (2011) arXiv:1111.2736
6. M. Vietri, *Astrop. J.* **453**, 883 (1995)
7. E. Waxman *et al.*, *Nuc. Ph. B* **118**, 353 (2003)
8. J.K. Becker *et al.*, *Astrop. Ph.* **25**, 118 (2006)
9. D. Guetta *et al.*, *Astrop. Ph.* **20**, 429 (2004)
10. E. Waxman *et al.*, *Phys. Rev. Lett.* **78**, 2292 (1997)
11. R. Abbasi *et al.*, *Nature* **484**, 351 (2012)
12. R. Abbasi *et al.*, *Astron. & Astroph.* **539**, A60 (2012)
13. S. Ando *et al.*, *Phys. Rev. Lett.* **95**, 061103 (2005)
14. J. Ahrens *et al.*, *Phys. Rev. D* **66**, 032006 (2002)
15. R. Abbasi *et al.*, *Phys. Rev. D* **85**, 042002 (2012)
16. R. Abbasi *et al.*, *Phys. Rev. D* **84**, 022004 (2011)
17. R. Abbasi *et al.*, ICRC (2011) arXiv:1111.2735
18. A.H. Compton *et al.*, *Phys. Rev.* **47**, 817 (1935)
19. A.A. Abdo *et al.*, *Astrop. J.* **698**, 2121 (2009)
20. M. Amenomori *et al.*, *Science* **314**, 439 (2006)
21. R. Abbasi *et al.*, *Astrop. J.* **718**, L194 (2010)
22. R. Abbasi *et al.*, *Astrop. J.* **740**, 16 (2011)
23. H. Falcke *et al.*, *Nature* **435**, 313 (2005)
24. T. Huege *et al.*, *Astrop. Ph.* **27**, 392 (2007)
25. O. Scholten *et al.*, *NIM A* **604**, S24 (2009)
26. K. de Vries *et al.*, *Astrop. Ph.* **34**, 267 (2010)
27. S. Böser *et al.*, *NIM A* **662**, 66 (2012)
28. P. Allison *et al.*, *Astrop. Ph.* **35**, 457 (2012)